Photoelectron Spectroscopy of Cobalt Oxide Cluster Anions

Axel Pramann, Kiichirou Koyasu, and Atsushi Nakajima*

Department of Chemistry, Faculty of Science and Technology, Keio University, 3-14-1 Hiyoshi, Kohoku-ku, Yokohama 223-8522, Japan

Koji Kaya

Institute of Molecular Science, Myodaiji, Okazaki 444-8585, Japan

Received: January 25, 2002

Photoelectron spectroscopy of size-selected $Co_nO_m^-$ clusters ($n = 4-20$; $m = 0-2$) is performed in a pulsed molecular beam experiment at photon energies of 3.49 and 4.66 eV. Cobalt oxide cluster anions are generated in a laser vaporization source and the photoelectron spectra are measured with a magnetic bottle photoelectron spectrometer. The size-dependent evolution of the electronic structure of the oxide clusters is discussed in terms of cluster composition. Threshold binding energy features are mainly contributed from Co d-derived orbitals throughout the complete series, indicating that the incoming oxygen atoms cause a minor influence on the electronic structures. Although for $n \geq 13$ EAs and VDEs of Co_n and Co_nO_m clusters overlap within the experimental resolution, at smaller cluster sizes, the values increase in the order of $Co_n < Co_nO < Co_nO_2$. For $Co_4O_3^-$ and $Co_5O_3^-$, the spectra indicate the presence of isomers with low EAs as peroxo and ozonide isomers. To compare the different channels of oxygen chemisorption, relative dissociation energies are determined via thermochemical cycles.

1. Introduction

Transition metal oxides have gained increasing interest in the last years.[1−4] This is based on the prominent role which transition metal oxides play in daily life: environmental processes such as surface corrosion but also phenomena in astrophysics, high-temperature chemistry, and many other fields of materials sciences exhibit an increasing importance.[2,3] However, a detailed understanding of these properties is still lacking. One of the most promising applications of transition metal oxides is their widespread use in heterogeneous catalysis because of their high selectivity and activity.[4] Therefore, the knowledge about the microscopic physical and chemical properties of cobalt oxides is of great importance.

Cluster science is a suitable tool for the study of physical and chemical properties such as electronic and geometric structures, reactivity, and dynamics on a microscopic level as a function of size and composition starting from the atom toward bulk phase. Therefore, transition metal oxide clusters provide a class of highly dispersed matter, which is able to model a catalyst on a microscopic scale with a clear and defined size. In the recent past, a limited number of spectroscopic studies have been performed on transition metal oxide clusters (see, for example, refs 5−13).

Cobalt and its oxides play an important role in industrial processes such as the formation of hydrocarbons from methane[14] or as promoters which can substantially increase the turnover number of catalytic reactions. Although bulk phase properties of cobalt oxides are well studied,[1,15−17] especially those of CoO which is the most stable cobalt oxide, a magnetic insulator with Co in the +2 ($3d^7$) oxidation state,[1] only few spectroscopic investigations have been performed on small cobalt oxide molecules.[18−20] Among the few studies on cobalt oxide clusters, Jacobson and Freiser have performed Fourier transform mass spectrometry on the reaction of cationic Co dimers and trimers with O_2.[21] This was followed by a kinetic study of the reaction of small Co_n^+ clusters ($n = 2-9$) with O_2 carried out by Castleman and co-workers using a selected ion drift tube with laser vaporization (SIDT-LV).[22] Rosen and co-workers determined the reactivity behavior of neutral Co_n clusters ($n = 10-60$) toward O_2 using a single-collision experiment.[23] The only investigation on cobalt oxide cluster anions has been performed by Kapiloff and Ervin who studied the reaction kinetics of small Co_n^- clusters ($n = 2-8$) toward O_2 using a flow tube experiment.[24]

Anion photodetachment photoelectron spectroscopy (PES) provides a state-of-the-art method to probe the electronic structure of the corresponding neutral clusters in the framework of the one particle approximation with the merits of mass separation.

In this article, we present the first investigation of mass-selected cobalt oxide cluster anions $Co_nO_m^-$ ($n = 4-20$; $m = 0-2$) using photodetachment photoelectron spectroscopy (PES) at 3.49 and 4.66 eV photon energies. The evolution of the electronic structure is studied in terms of cluster size and composition, and electron affinities (EAs) and first vertical detachment energies (VDEs) are determined. The electronic structures of the oxides are compared to those of the corresponding pure Co_n^- clusters, which we have measured under the same experimental conditions. The influence of increasing oxygen content *m* and cluster size *n* is discussed. The motivation of this study is to get a first insight into oxygen chemisorption principles and the nature of chemical bonding between Co and oxygen with an increasing number of O atoms on a microscopic level. Additionally, relative dissociation energies are determined for main oxygen fragmentation channels, which simulate the energetics of the dissociative loss of one oxygen atom or an oxygen dimer from the intact parent cluster.

* To whom correspondence should be addressed. Fax: +81-45-566-1697. E-mail: nakajima@sepia.chem.keio.ac.jp.

10.1021/jp020247d CCC: $22.00
Published on Web 04/19/2002

2. Experimental Section

Details of the experimental apparatus and the applied procedures have been reported elsewhere.[25] Here, we will give only a brief description. $Co_nO_m^-$ clusters are generated with the aid of a pulsed laser vaporization cluster source. The light of the second harmonics output (2.33 eV, 532 nm) of a Nd^{3+}:YAG laser (10 Hz repetition rate, 25 mJ pulse energy) is focused onto a translating and rotating cobalt rod (5 mm diameter; 99.999% purity). The generated plasma is cooled by a helium pulse (stagnation pressure: 10 atm), and cluster formation occurs by plasma reactions between cobalt and oxygen atoms. The latter originate from residual surface layers of oxygen on the cobalt target rod. No additional oxygen is mixed with the carrier gas in order to guarantee a mild oxidation with a minor content of oxygen in the respective cluster composition. After a supersonic expansion, cluster anions are mass-separated by their time-of-flight and mass-analyzed by an in-line time-of-flight mass spectrometer (TOF-MS) with a resolution $m/\Delta m = 230$. After deceleration, the cluster anions are irradiated with a Q-switched Nd^{3+}:YAG laser operating at 3.49 and 4.66 eV photon energy (laser fluence: 5−20 and 1−3 mJ/cm^2, respectively). The kinetic energy of the detached photoelectrons is measured with a magnetic bottle type photoelectron spectrometer (TOF−PES).[26−29] The binding energy spectra are obtained by subtracting the kinetic energy from the photon energy. Each spectrum is measured by accumulating 10 000−30 000 experimental runs at 10 Hz repetition rate. The resolution of the electron spectrometer is better than 50 meV at 1 eV kinetic energy (eKE) and decreases according to $(eKE)^{3/2}$ at higher binding energies. Generally, lower photon energies yield higher resolved spectra, whereas higher photon energies cover a broader spectral range. The calibration of the machine is performed using the strong ground-state transition line ($^1S_0 \rightarrow 2S_{1/2}$) of the gold atomic anion.[30] During the experiments, no laser power dependent spectral changes are observed, and fragmentation processes can be excluded.

3. Results and Discussion

A. Mass Spectra of Cobalt Oxide Cluster Anions. Figure 1 shows a typical time-of-flight mass spectrum of negatively charged cobalt oxide clusters $Co_nO_m^-$ ($n = 3-25$; $m = 0-3$) generated with a conventional laser vaporization cluster source by plasma reactions between oxygen resulting from the target rod surface and cobalt using a nonseeded pure helium carrier gas. Generally, the cluster ion intensities show the following sequence: $Co_nO^- > Co_n \rightarrow Co_nO_2 \rightarrow Co_nO_3^-$. For $n < 8$, the intensities of the corresponding monoxides overcome those of the pure Co_n^- clusters by a factor of 1.2−2.2. This is a primary indication of higher electron affinities of monoxide clusters compared to pure clusters especially in the small size region below $n = 8$. The high abundance of Co_5O^- cannot be explained using the principles of redox chemistry: assuming an oxidation state of −2 of the oxygen atom and the most stable oxidation state of +3 of the Co atom which has an $[Ar]3d^74s^2$ valence electron configuration should lead to a most stable stoichiometric composition of $Co_5O_8^-$ in the case of the Co pentamer core. Thus, the current conditions for oxide formation can be described as mild and kinetically dominated. Furthermore, the high intensities of the monoxides reveal dissociative chemisorption of oxygen as the major reaction channel compared to molecular adsorption under these experimental conditions. This behavior is most probably directly related to the high binding energy of Co−O which is 384.5 kJ/mol.[31] However, this binding energy is valid only for the diatomic molecule and not necessarily for the Co cluster. The inset of Figure 1 shows the $Co_nO_m^-$ distribution for $n = 9$ and 10 in more detail. Because of the low intensities of larger oxides ($m \geq 3$), the monoxide and dioxide clusters are mainly investigated in this study. The mass spectrometric distribution of $Co_nO_m^-$ clusters in the present study differs strongly from that obtained by Ervin and coworkers.[24] This is probably due to the fact of a different cluster generation method under thermal conditions in the latter work.

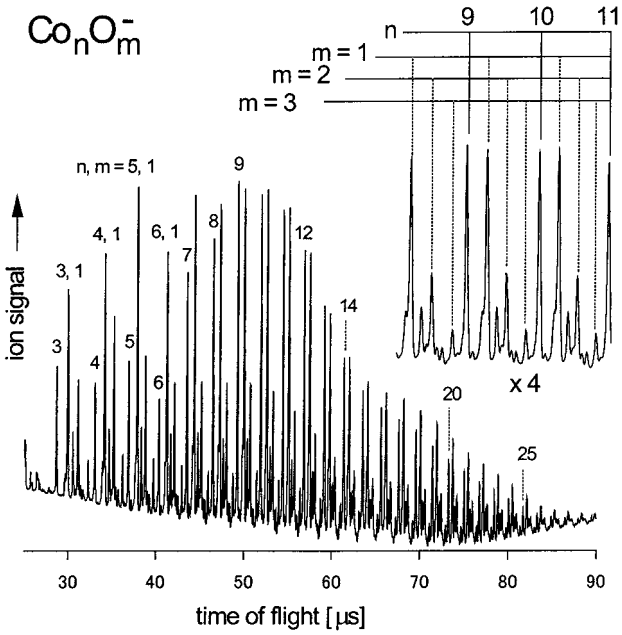

Figure 1. Typical time-of-flight mass spectrum of $Co_nO_m^-$ clusters ($n = 3-25$; $m = 0-3$). The oxide clusters are generated by plasma reactions of oxygen traces on the Co target surface and the Co target plasma itself. The order of intensities is $Co_nO^- > Co_n^- > Co_nO_2^- > Co_nO_3^-$.

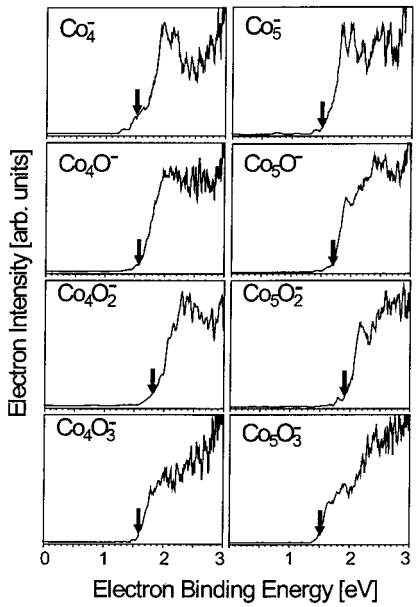

Figure 2. Photoelectron spectra of $Co_nO_m^-$ ($n = 4, 5$; $m = 0-3$) taken at 355 nm. Vertical arrows indicate electron affinities.

B. Photoelectron Spectroscopy of Cobalt Oxide Cluster Anions. The photoelectron spectra of Co_n^- and $Co_nO_m^-$ clusters ($n = 4-20$; $m = 0-2$) were measured using 3.49 and 4.66 eV photon energies, and are displayed in Figures 2−4. The smaller size regime ($n < 6$) is probed by the third harmonics output (355 nm) of the detachment laser in order to get a better

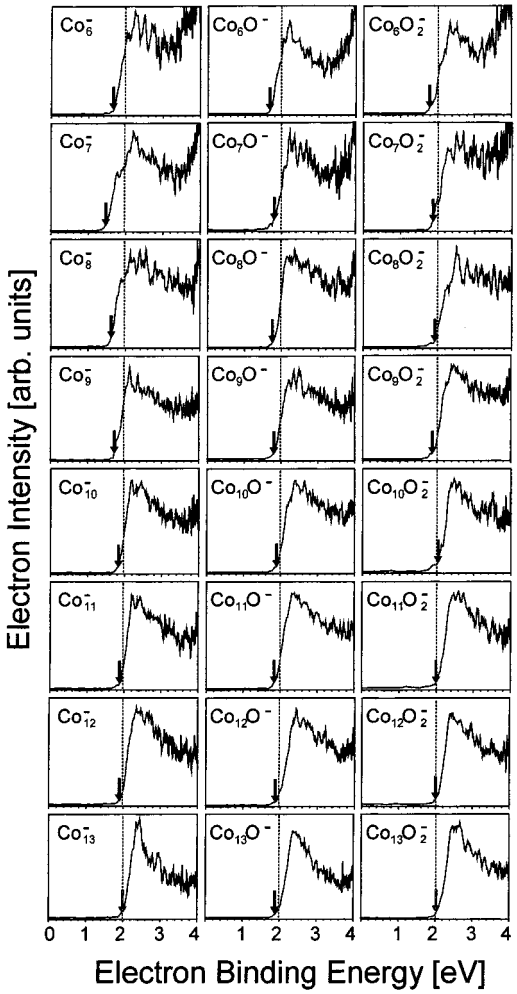

Figure 3. Photoelectron spectra of $Co_nO_m^-$ ($n = 6-13$; $m = 0-2$) taken at 466 nm.

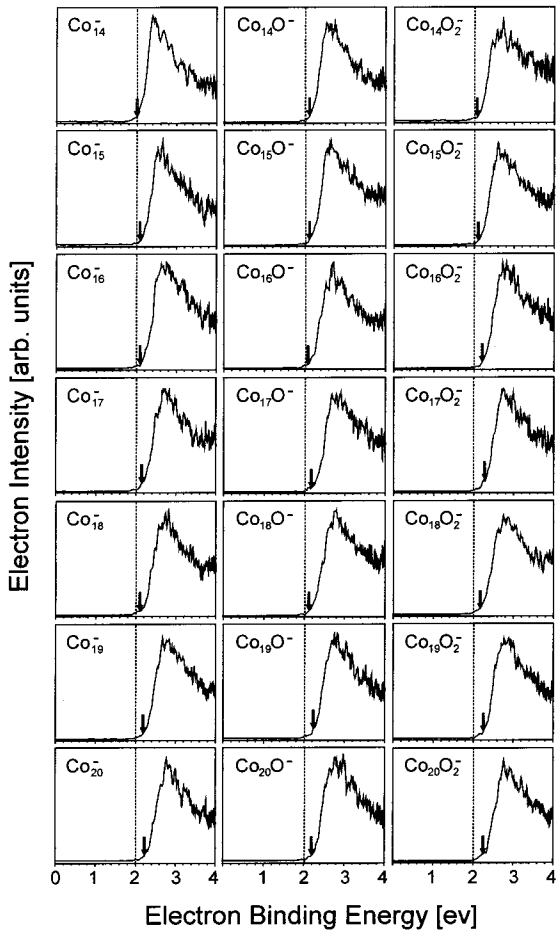

Figure 4. Photoelectron spectra of $Co_nO_m^-$ ($n = 14-20$; $m = 0-2$) taken at 466 nm.

resolution of low lying electronic states, whereas for clusters with $n \geq 6$, a detachment energy of 4.66 eV is applied to unveil the evolution of the electronic structure toward the bulk. Generally, the application of the one particle approximation for the detachment process $Co_nO_m + e^- \leftarrow Co_nO_m^-$ reveals the electronic transitions from the ground state of the precursor anion to the respective ground or excited states of the neutral in the geometry of the anion. Spectral broadening at the threshold region often indicates a geometric change between the anionic and the neutral clusters. From the photoelectron spectra, the threshold binding energies (ETs) are directly determined as upper limits of adiabatic electron affinities (EAs) by using the onset of the respective photoelectron spectra at 10% of the first peak maximum. For convenience, we treat the ET values as EAs. The shape of the first peak (the onset) is important for a correct assignment of the EA, because the adiabatic EAs can only be determined if the $0 \leftarrow 0$ transition can be resolved. The more sharp the onset, the more accurate the EAs can be determined. We have additionally determined vertical detachment energies (VDEs) from the first maxima of the photoelectron spectra. The EA and VDE values of Co_nO_m clusters are shown in Figure 5.

B.1. Photoelectron Spectra of $Co_4O_m^-$ and $Co_5O_m^-$ ($m = 0-3$). In Figure 2, the photoelectron (PE) spectra of $Co_nO_m^-$ ($n = 4, 5$; $m = 1-3$) measured at 3.49 eV are displayed together with those of the corresponding pure Co_n^- clusters. We have measured the PE spectra of pure Co_n^- clusters under the same experimental conditions to provide a direct comparison with those of $Co_nO_m^-$ clusters. Generally, within the experimental error, the PE spectra of pure Co_n^- clusters are in agreement with those reported in refs 32 and 33. Moreover, the latter work provides highly resolved PE spectra. The Co tetramer cluster and its oxides are the smallest species we are able to study under the current experimental conditions. Even when the mass spectrum in Figure 1 reveals a considerable intensity of the trimer and its oxides, their low photodetachment cross sections provide a very poor signal-to-noise ratio. The spectral features of Co_4O^-, $Co_4O_2^-$, and $Co_4O_3^-$ show a general broadening because of the hybridization of energetically higher O 2p and Co 3d-derived states. Whereas the low binding energy features of pure Co_n^- clusters are dominated from low lying 3d-derived electronic states, the corresponding oxide spectra reveal some influence of the oxygen 2p and 2p-derived orbitals, which merge with the 3d states of the Co cluster. In the case of the monoxide and dioxide, the threshold energies shift slightly toward higher values together with the first VDEs. In the case of the $Co_4O_3^-$ cluster the EA decreases again. This decrease may imply the appearance of a peroxo or ozonide isomer with a lower electron affinity, because after varying the source conditions the slope of the threshold onset for $Co_4O_3^-$ apparently changes. In the right column of Figure 2, the PE spectra of the pentamer series are displayed. Compared to the $Co_4O_m^-$ clusters, the course of the threshold energies is similar. Especially, the EA of the $Co_5O_3^-$ cluster is also shifted to a smaller value, and also, this low energy feature changes with the source conditions, indicating the presence of an isomer. With an increasing number of Co atoms, the spectral features become more structureless which is a result of the marked influence of Co 3d-derived electronic

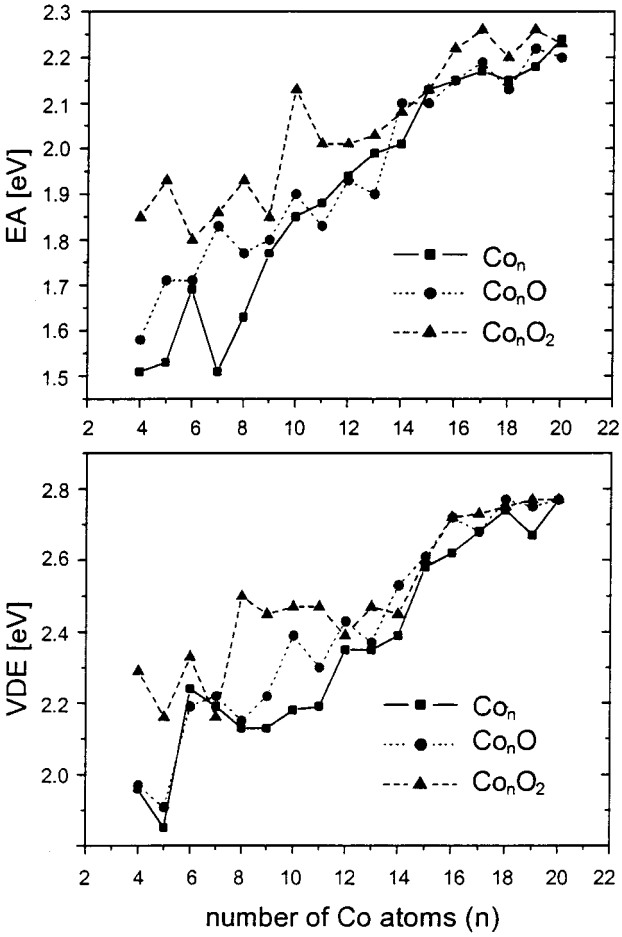

Figure 5. Upper plot: electron affinities (EAs) of Co_n (filled squares), Co_nO (filled circles), and Co_nO_2 (filled triangles). For more clarity, error bars which are in the range of 100−200 meV are not displayed. Lower plot: vertical detachment energies (VDEs) of Co_n (filled squares), Co_nO (filled circles), and Co_nO_2 (filled triangles).

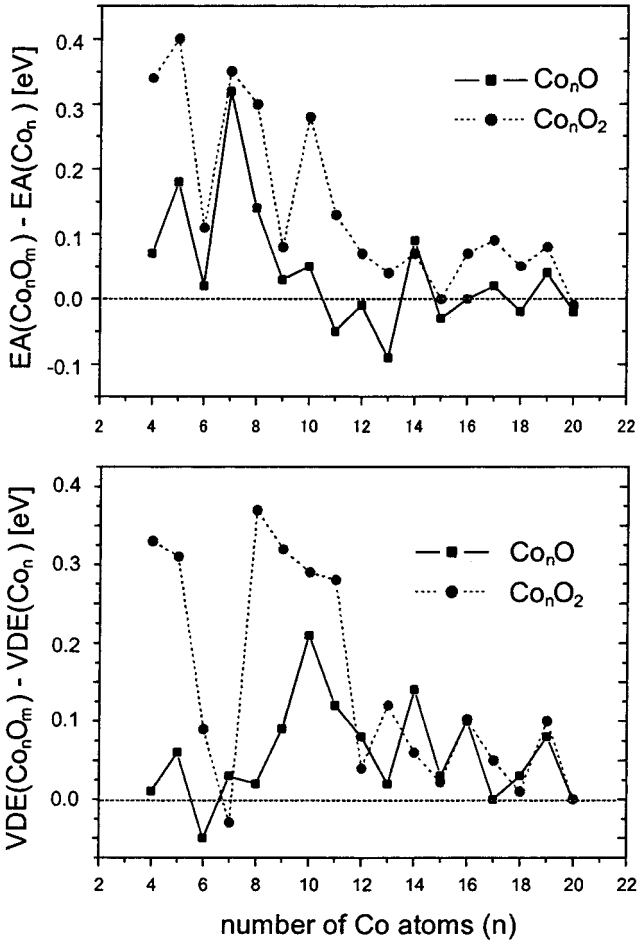

Figure 6. Differences (shifts) of electron affinities (upper plot) and vertical detachment energies (lower plot) between Co_nO_m and pure Co_n. The horizontal line indicates a ΔEA or ΔVDE = 0.

states. The additional sharp peak (first VDE) in the $Co_5O_2^-$ spectrum emphasizes a stable Co-O bonding after dissociative chemisorption of O_2. In the case of $Co_5O_3^-$, the presence of isomers and less rigid structures lowers the threshold energy. In Figure 6, the differences of EAs and VDEs between the cobalt oxide clusters and pure cobalt clusters are displayed to investigate the energy shift induced by the increasing degree of oxidation of the pure Co_n precursor clusters. For the tetramer, the monoxides reveal only small energy differences (ΔEA, ΔVDE < 100 meV), whereas the dioxides exhibit a larger energy shift. For the pentamer, a similar behavior can be observed.

B.2. Photoelectron Spectra of $Co_nO_m^-$ (n = 6−13; m = 0−2). Figure 3 shows the photoelectron spectra of $Co_nO_m^-$ clusters (n = 6−13; m = 0−2) measured at 4.66 eV photon energy. For $n \geq 6$, only the monoxides and dioxides are investigated because of a lower mass abundance of higher oxides. Electron affinities are indicated by downward arrows and displayed with VDEs in Figure 5. Generally, threshold energies shift to higher values from n = 6 to 14 (see, for example, EA (Co_6O) = 1.71 eV and EA ($Co_{14}O$) = 2.10 eV), though they still show size dependence especially at smaller cluster sizes. Most spectra reveal a similar shape. In a former study for the electronic structure of small yttrium oxide clusters, $Y_nO_m^-$, recently performed in our group,[13] the spectra exhibit more structural features, and main electronic transitions are separated more clearly. This is a consequence of the valence electron configuration of the Y atom which has only one electron more localized in the 4d orbital. In the case of $Co_nO_m^-$ clusters, however, the 3d orbital is occupied by seven electrons. This electron-rich configuration causes a huge variety of electronic states and spin coupling effects. However, this is only related to the electron configuration of the atom. The $Co_nO_m^-$ spectra are dominated by a strong peak evolving around the threshold binding energy. The origin of this feature can be attributed to the 3d-derived electronic states of the pure Co_n^- clusters. With few exceptions, the order of EAs is $Co_n < Co_nO < Co_nO_2$. The origin of the higher EAs of dioxides can be derived from the nature of a strong dioxide bonding within the cluster framework. Generally, the influence of oxygen atoms toward the electronic structure gradually becomes less prominent at a larger size n. This is a consequence of the nearly bulklike electronic structure at this size range, which is dominated by the Co contribution. In Figure 6, the energy shift of EAs and VDEs between the cobalt oxide clusters and pure cobalt clusters exhibits some size dependent variations. The EA shift is larger for the dioxides with maxima at n = 7 and 10, whereas the monoxides show a maximum at 7 and 14. However, there are some conspicuous size-dependent maxima in the energy shifts, indicating a strong influence of the incoming oxygen toward the electronic structure of the respective cluster.

B.3. Photoelectron Spectra of $Co_nO_m^-$ (n = 14−20; m = 0−2). The photoelectron spectra of $Co_nO_m^-$ (n = 14−20; m = 0−2) measured at 4.66 eV photon energy are displayed in Figure 4. The EAs and VDEs are plotted in Figure 5. When these spectra are compared, it is evident that all spectra reveal very

similar electronic features: an intense peak centered near the threshold together with a relatively sharp onset. The latter implies a rather rigid geometrical structure of both the anion and the neutral cluster, revealing a closedly packed structure. With increasing cluster size, EAs and VDEs increase, and those of the pure Co_n clusters, their monoxides, and dioxides almost overlap within the experimental resolution. As shown in Figure 6, the EA and VDE shifts in the monoxides, dioxides, and pure Co_n are in the range of 100 meV which is comparably smaller than for $n < 15$. Therefore, the main electronic structure contribution in this size range originates from the Co atoms. The transition from molecular to metallic-like electronic structures occurs at very small cluster sizes, and a value of $n = 7$ is reported in ref 32) after applying the spherical conducting droplet (csd) model.

B.4. Relative Dissociation Energies: Pathways for Dissociative and Molecular Chemisorption. The measurement of EAs enables us to estimate dissociation energies for the negatively charged clusters if the dissociation energies of the corresponding neutral clusters are known. This can be performed using simple thermochemical cycles. In our work, we determined relative dissociation energies, which are the differences of the dissociation energies between the anion cluster and the corresponding neutral. These differences are related to the following three chemisorption processes of oxygen on the cluster surface:

$$Co_nO^- \rightarrow Co_n^- + O \quad (1)$$

$$D_0(Co_n^- - O) - D_0(Co_n - O) = EA(Co_nO) - EA(Co_n) \quad (1a)$$

$$Co_nO_2^- \rightarrow Co_n^- + O_2 \quad (2)$$

$$D_0(Co_n^- - O_2) - D_0(Co_n - O_2) = EA(Co_nO_2) - EA(Co_n) \quad (2a)$$

$$Co_nO_2^- \rightarrow Co_nO^- + O \quad (3)$$

$$D_0(Co_nO^- - O) - D_0(Co_nO - O) = EA(Co_nO_2) - EA(Co_nO) \quad (3a)$$

Using these relations, it is possible to gain some insight into relative energy barriers for the oxygen intercalation or oxygen-loss into or from the cluster. In the case of cobalt oxide clusters, the above three most reasonable dissociation pathways are investigated: the loss of an oxygen atom from the monoxide cluster, the loss of an oxygen molecule from the dioxide, and the fragmentation of the dioxide into a negatively charged monoxide and an oxygen atom. These processes should be energetically favored, because the EAs of the pure and monoxide clusters are higher than those of atomic and molecular oxygen. The electron affinity of atomic oxygen is 1.461 eV,[34] and that of the O_2 molecule is 0.451 eV.[35] Using these values and eqs 1a, 2a, and 3a, we calculated the relative dissociation energies (ΔD_0), which are plotted in Figure 7. With increasing cluster size, these differences decrease ranging around 100 meV for $n > 10$. When the ΔD_0 values are positive, they indicate a higher dissociation energy and stability of the respective anion cluster.

4. Conclusions

Anion photoelectron spectroscopy of mass-selected $Co_nO_m^-$ clusters ($n = 4-20$; $m = 0-2$) is performed at photon energies of 3.49 and 4.66 eV. The size-dependent evolution of the electronic structure of the $Co_nO_m^-$ clusters is discussed in terms of composition and, furthermore, compared to that of pure Co_n^- clusters. EAs and first VDEs are determined. Main spectral features are contributed from Co 3d-derived orbitals throughout the complete series. The additional oxygen atoms indicate a minor influence toward the electronic structure. With increasing oxygen content, electron affinities shift to higher values. The most prominent feature appears at Co_{13}^-, which indicates a rigid geometric structure of an icosahedron with I_h symmetry.[33] For $n > 12$, EAs and VDEs of Co_n and Co_nO_m clusters overlap within the experimental resolution, whereas at smaller cluster sizes, EAs increase in the order $Co_n < Co_nO < Co_nO_2$. Additionally, relative dissociation energies, which are defined as the differences of the dissociation energies between the anion clusters and the corresponding neutral clusters, are investigated showing a higher dissociation energy and stability of the anion cluster. A larger ΔD_0 value for the oxygen dimer loss channel reveals a higher stability of the anionic dioxide than the anionic monoxide compared to their neutrals.

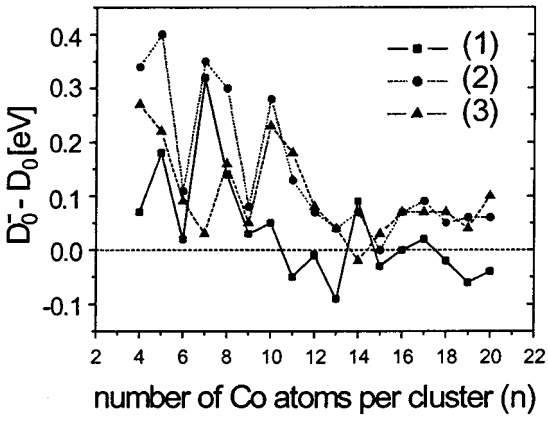

Figure 7. Relative dissociation energies for oxygen-loss channels. (1) loss of O from Co_nO (eq 1a), (2) loss of O_2 from Co_nO_2 (eq 2a), and (3) loss of O from Co_nO_2 (eq 3a).

Acknowledgment. This work is supported by a program entitled "Research for the Future (RFTF)" of the Japan Society for the Promotion of Science (98P01203) and by a Grant-in-Aid for scientific research (C) (No. 13640582) from the Ministry of Education, Science, Sports and Culture. A.P. gratefully acknowledges a postdoctoral fellowship from the Japan Society for the Promotion of Science (JSPS).

References and Notes

(1) Henrich, V. E.; Cox, P. A. *The Surface Science of Metal Oxides*; Cambridge University Press: New York, 1994.
(2) Rao, C. N. R. *Annu. Rev. Phys. Chem.* **1989**, *40*, 291.
(3) Merer, A. J. *Annu. Rev. Phys. Chem.* **1989**, *40*, 407.
(4) Transition Metal Oxides: Surface Chemistry and Catalysis. *Studies in Surface Science and Catalysis*; Kung, H. H., Ed.; Elsevier: Amsterdam, The Netherlands, 1989; Vol. 45.
(5) Knickelbein, M. B. *J. Chem. Phys*. **1995**, *102*, 1.
(6) Yang, S.; Knickelbein, M. B. *Z. Phys. D* **1994**, *31*, 1999.
(7) Wu, H.; Wang, L.-S. *J. Chem. Phys.* **1997**, *107*, 16.
(8) Wu, H.; Wang, L.-S. *J. Chem. Phys*. **1997**, *107*, 8221.
(9) Wu, H.; Wang, L.-S. *J. Chem. Phys.* **1998**, *108*, 5310.
(10) Thomas, O. C.; Xu, S.-J.; Lippa, T. P.; Bowen, K. H., Jr. *J. Cluster Sci.* **1999**, *10*, 525.
(11) Klingeler, R.; Luettgens, G.; Pontius, N.; Rochow, R.; Bechthold, P. S.; Neeb, M.; Eberhardt, W. *Eur. Phys. J. D* **1999**, *9*, 263.
(12) Pramann, A.; Rademann, K. *Chem. Phys. Lett.* **2001**, *343*, 99.
(13) Pramann, A.; Nakamura, Y.; Nakajima, A.; Kaya, K. *J. Phys. Chem. A* **2001**, *105*, 7534.
(14) Haggin, J. *Chem. Eng. News* **1991**, *April 29*, 22−24.
(15) Langell, M. A.; Anderson, M. D.; Carson, G. A.; Peng, L.; Smith, S. *Phys. Rev. B* **1999**, *59*, 4791.

(16) Castell, M. R.; Dudarev, S. L.; Briggs, G. A. D.; Sutton, A. P. *Phys. Rev. B* **1999**, *59*, 7342.

(17) Reddy, E. P.; Rojas, T. C.; Sanchez-Lopez, J. C.; Dominguez, M.; Roldan, E.; Campora, J.; Palma, P.; Fernandez, A. *Nanostruc. Mat*. **1999**, *12*, 61.

(18) Clouthier, D. J.; Huang, G.; Merer, A. J.; Friedman-Hill, E. J. *J. Chem. Phys.* **1993**, *99*, 6336.

(19) Van Zee, R. J.; Hamrick, Y. M.; Li, S.; Weltner, W., Jr. *J. Phys. Chem*. **1992**, *96*, 7247.

(20) Chertihin, G. V.; Citra, A.; Andrews, L.; Bauschlicher, C. W., Jr. *J. Phys. Chem. A* **1997**, *101*, 8793.

(21) Jacobson, D. B.; Freiser, B. S. *J. Am. Chem. Soc*. **1986**, *108*, 27.

(22) Guo, B. C.; Kerns, K. P.; Castleman, A. W., Jr. *J. Phys. Chem*. **1992**, *96*, 6931.

(23) Andersson, M.; Persson, J. L.; Rosen, A. *J. Phys. Chem*. **1996**, *100*, 12222.

(24) Kapiloff, E.; Ervin, K. M. *J. Phys. Chem. A* **1997**, *101*, 8460.

(25) Nakajima, A.; Taguwa, T.; Hoshino, K.; Sugioka, T.; Naganuma, T.; Ono, F.; Watanabe, K.; Nakao, K.; Konishi, Y.; Kishi, R.; Kaya, K. *Chem. Phys. Lett*. **1993**, *214*, 22.

(26) Kruit, P.; Read, F. H. *J. Phys. E* **1983**, *16*, 313.

(27) Cheshnovsky, O.; Yang, S. H.; Pettiette, C. L.; Craycraft, M. J.; Smalley, R. E. *Rev. Sci. Instrum.* **1987**, *58*, 2131.

(28) Gantefoer, G.; Meiwes-Broer, K. H.; Lutz, H. O. *Phys. Rev. A* **1988**, *37*, 2716.

(29) Handschuh, H.; Gantefoer, G.; Eberhardt, W. *Rev. Sci. Instrum*. **1995**, *66*, 3838.

(30) Hotop, H.; Lineberger, W. C. *J. Phys. Chem. Rev. Data* **1975**, *4*, 539.

(31) *Handbook of Chemistry and Physics*, 80th ed.; Lide, D. R., Ed.; CRC Press: Boca Raton, FL, 1999−2000.

(32) Yoshida, H.; Terasaki, A.; Kobayashi, K.; Tsukada, K.; Kondow, T. *J. Chem. Phys.* **1995**, *102*, 5960.

(33) Liu, S.-R.; Zhai, H.-J.; Wang, L.-S. *Phys. Rev. B* **2001**, *64*, 153402.

(34) Hotop, H.; Lineberger, W. C. *J. Phys. Chem. Rev. Data* **1985**, *14*, 731.

(35) Travers, M. J.; Cowles, D. C.; Ellison, G. B. *Chem. Phys. Lett.* **1989**, *164*, 449.